

Quasiparticle scattering and local density of states in the d -density wave phase

Cristina Bena,¹ Sudip Chakravarty,² Jiangping Hu,² and Chetan Nayak²

¹*Department of Physics, University of California at Santa Barbara, Santa Barbara, CA 93106, USA*

²*Department of Physics and Astronomy, University of California Los Angeles, Los Angeles, California 90095-1547, USA*
(Dated: November 15, 2018)

We study the effects of single-impurity scattering on the local density of states in the high- T_c cuprates. We compare the quasiparticle interference patterns in three different ordered states: d -wave superconductor (DSC), d -density wave (DDW), and coexisting DSC and DDW (DSC-DDW). In the coexisting state, at energies below the DSC gap, the patterns are almost identical to those in the pure DSC state with the same DSC gap. However, they are significantly different for energies greater than or equal to the DSC gap. This transition at an energy around the DSC gap can be used to test the nature of the superconducting state of the underdoped cuprates by scanning tunneling microscopy. Furthermore, we note that in the DDW state the effect of the coherence factors is stronger than in the DSC state. The new features arising due to DDW ordering are discussed.

PACS numbers: 05.30.Fk, 03.75.Nt, 71.10.Fd, 02.70.Ss

I. INTRODUCTION

One of the intriguing features of the cuprate high temperature superconductors is the existence of a pseudogap phase in the normal state.¹ Elucidating the nature of the pseudogap would be an important step in understanding the physics of high-temperature superconductivity. Among many scenarios, one concrete proposal is that the pseudogap is due to a hidden broken symmetry² of $d_{x^2-y^2}$ type in the particle-hole channel.³ In this paper we examine the consequences of the presence of DDW ordering on the quasiparticle interference patterns observed by scanning tunneling measurements (STM).

Recently, interesting STM measurements^{4,5,6} on Bi-2122 have been performed to obtain Fourier transformed spectra of the local density of states. This technique is called Fourier transform scanning tunneling spectroscopy (FT-STs). So far, the experiments have been carried out in the superconducting state at low temperatures, and the results can be interpreted as interference patterns due to elastic scattering of the quasiparticles from impurities.^{4,7,8,9} Additional support of this interpretation comes from a more recent work in Ref. 10. The scattering of quasiparticles between regions of the Brillouin zone with high densities of states yields peaks in FT-STs. In a d -wave superconductor (DSC), the regions of high local density of states (LDOS) are situated at the tips of the banana-shaped contours of the quasiparticle excitation spectrum.⁴ The wavevectors of the observed peaks are consistent with the wavevectors that connect the tips of these bananas (see Fig.1). Thus, the experimental results are consistent with the known pictures of the Fermi surface and the LDOS in the pure DSC state. Here, we investigate the possible form of STM spectra in both the superconducting and normal states from the perspective of DDW. The T-matrix formalism,⁹ combined with a numerical analysis, are used to obtain the quasiparticle interference patterns of the various ordered states.

We first consider a pure DSC state and recover results similar to Ref. 9. Though the band structure we used

is different from theirs, the main features such as the emergence of peaks at particular wave vectors are still observed. However, as we will discuss later, differences in the band structure can have large effects on the details of the STM spectra, especially due to coherence factors. Fortunately, none of our robust qualitative conclusions depend on the spurious sensitivity to the band structure.

Our main focus is to study the mixed, or coexisting, DSC-DDW and the pure DDW states. According to the DDW theory,² the mixed DSC-DDW and the pure DDW characterize the underdoped superconducting and the pseudogap phase respectively. We first analyze the mixed state and find that if we probe the system at energies larger than the DSC gap, significant differences among the interference patterns emerge compared to a pure DSC state, while at energies below the DSC gap, the patterns are almost identical. For example, let us focus on the position of the peaks along the (π, π) direction in the interference patterns. For a pure DSC state they should move away from the origin with increasing energy and eventually get close to the (π, π) point for energies of the order of the gap. If the state is a mixed state (DSC-DDW) with two different order parameters, the total gap is roughly equal to the square root of the sum of the two gaps square. In this case the same peaks should shift away from the origin faster (for lower energy) and get close to the (π, π) point at energies of the order of the DSC gap which is typically much smaller than the total gap. For energies larger than the DSC gap, the main features of the STM spectra is significantly different from those in the pure DSC state. Therefore, the energy of the DSC gap in the mixed states marks a transition in the interference patterns. The effect becomes less pronounced with an increase in doping, as the DSC gap is getting closer to the total gap of the system. Based on this observation we believe that the FT-STs obtained below the superconducting transition temperature in the underdoped cuprates may reveal important information about the nature of the order parameter.

In the pure DDW state, the interference patterns re-

veal features similar to the ones observed in the DSC state and others that are entirely new. These features could be used to detect DDW order. One of the important differences from the case of DSC order is that the DOS is not as strongly peaked in the DDW state, so the STM spectrum is more strongly dependent on coherence factors. These depend not only on the order parameter and on the band structure, but also on the details of the scattering and on the type of impurities. We illustrate this effect by comparing the interference patterns for two parameter sets which are identical save for the sizes of their DDW gaps. Changing the size of the DDW gap has relatively little effect on the equal energy contour plots. However, the interference patterns are dramatically different due to the difference in the coherence factors. The authors of Ref. 11 emphasized their importance. We show that their observation is pertinent and, in fact, explains why their lowest-order Born approximation results miss some of the physics captured

in the full T-matrix approach. Also, the strong dependence of the STM spectra on coherence factors suggests that they could be used to extract detailed information about the DDW gap, band structure, etc., which could be compared with angle-resolved photoemission spectra (ARPES) data.

The paper is organized as follows. In section II we describe our model and the analytic formalism. In section III, we describe the numerical analysis and discuss the results; we conclude in section IV.

II. ANALYTIC FORMALISM

In the presence of DDW and DSC order, the general mean field Hamiltonian for a high T_c superconductor is given by

$$H = \sum_{k\sigma} [\epsilon(k) - \mu] c_{k\sigma}^+ c_{k\sigma} + \sum_k \left[\sum_{\sigma} iW(k) c_{k\sigma}^+ c_{k+Q,\sigma} + \Delta(k) c_{k\uparrow}^+ c_{-k\downarrow}^+ \right] + h.c. \quad (1)$$

where $W(k) = W_0(\cos k_x - \cos k_y)/2$ and $\Delta(k) = \Delta_0(\cos k_x - \cos k_y)/2$ are the DDW order (see also ref. 3) and DSC order parameters respectively, and $Q = (\pi, \pi)$. The sums over k include all the wave vectors in the first Brillouin zone (BZ), $|k_x| \leq \pi$, $|k_y| \leq \pi$. We take the lattice constant $a = 1$.

The kinetic energy is $\epsilon(k) = \epsilon_1(k) + \epsilon_2(k)$, where ϵ_1/ϵ_2 are respectively odd/even with respect to the shift of the wavevector by Q ; $\epsilon_1(k) = -\epsilon_1(k+Q)$ and $\epsilon_2(k) = \epsilon_2(k+Q)$. In the numerical calculation, we focus on a simple t, t' band structure with dispersion $\epsilon_1(k) = t(\cos k_x + \cos k_y)/2$ and $\epsilon_2(k) = t' \cos k_x \cos k_y$.

To simplify the calculation, we introduce a four-component (spinor) field operator, $\psi_k^+ = (c_{k\uparrow}^+, c_{k+Q\uparrow}^+, c_{-k\downarrow}, c_{-k-Q\downarrow})^{12}$. In this new basis, the above Hamiltonian can be written as

$$H = \sum_k \psi_k^+ A(k) \psi_k, \quad (2)$$

where k is summed over half of the original Brillouin zone (reduced Brillouin zone - RBZ), namely, $|k_x| + |k_y| \leq \pi$. A_k is a four by four matrix given by

$$A_k = \begin{pmatrix} \epsilon_1(k) + \epsilon_2(k) - \mu & iW(k) & \Delta(k) & 0 \\ -iW(k) & -\epsilon_1(k) + \epsilon_2(k) - \mu & 0 & -\Delta(k) \\ \Delta^*(k) & 0 & -\epsilon_1(k) - \epsilon_2(k) + \mu & iW(k) \\ 0 & -\Delta(k)^* & -iW(k) & \epsilon_1(k) - \epsilon_2(k) + \mu \end{pmatrix}. \quad (3)$$

The eigenvalues of A_k are $\pm E_1(k)$ and $\pm E_2(k)$, where

$$E_{1,2}(k) = \{(\sqrt{\epsilon_1(k)^2 + W(k)^2} \pm [\epsilon_2(k) - \mu])^2 + \Delta(k)^2\}^{\frac{1}{2}} \quad (4)$$

We consider impurity scattering of the form:

$$H_{\text{imp}} = \sum_{k,k'} \sum_{\alpha,\beta=\uparrow,\downarrow} V_{kk'\alpha\beta} c_{k\alpha}^+ c_{k'\beta} \quad (5)$$

Up to a constant, we can write it as

$$H_{\text{imp}} = \sum_{k,k' \in \text{RBZ}} \psi_k^+ V(k, k') \psi_{k'}, \quad (6)$$

where $V(k, k')$ is a four by four matrix.

One can define a finite temperature (imaginary time) Green's function,

$$G(k_1, k_2, \tau) = -\text{Tr} \left[e^{-\beta(K-\Omega)} \mathbf{T}_\tau \psi_{k_1}(\tau) \psi_{k_2}^\dagger(0) \right] \quad (7)$$

where $K = H - \mu N$, $e^{-\beta\Omega} = \text{Tr} e^{-\beta K}$, and \mathbf{T}_τ is the imaginary time ordering operator. The impurity scattering problem can be solved by computing the Fourier transform of the Green's function from the T -matrix for-

mulation :

$$G(k_1, k_2, i\omega_n) = G_0(k_1, i\omega_n) T(k_1, k_2, i\omega_n) G_0(k_2, i\omega_n), \quad (8)$$

where

$$G_0(k, i\omega_n)^{-1} = i\omega_n I - A_k, \quad (9)$$

I is the 4×4 identity matrix, and

$$T(k_1, k_2, i\omega_n) = V(k_1, k_2) + \sum_{k' \in \text{RBZ}} V(k_1, k') G_0(k', i\omega_n) T(k', k_2, i\omega_n). \quad (10)$$

For simplicity, we take the impurity scattering potential to be a delta function so that the matrix V is independent of k and k' ; $V(k, k') = V$. For this case, we can solve Eq. (10) and obtain

$$T(i\omega_n) = [1 - V \int dk G_0(k, i\omega_n)]^{-1} V \quad (11)$$

where the only difference from the standard result is that the integral over k is over the RBZ.

Consequently, the local density of states $\rho(q, \omega)$, is given by

$$\rho(q, \omega) \sim \frac{i}{2\pi} \sum_{k \in \text{RBZ}} g(k, q, \omega). \quad (12)$$

where $g(k, q, \omega)$ is defined as follows. Let $k' = k + q$. If k' is in the RBZ,

$$g(k, q, \omega) = \sum_{i=1}^4 [G_{ii}(k, k', s_i \omega) - G_{ii}^*(k', k, s_i \omega)] \quad (13)$$

where $s_i = 1$ for $i = 1, 2$ and $s_i = -1$ for $i = 3, 4$. If k' is not in the RBZ, let $k'' = k + q - Q$. For this case

$$g(k, q, \omega) = \sum_{i=1,3} [G_{i,i+1}(k, k'', s_i \omega) - G_{i,i+1}^*(k'', k, s_i \omega) + G_{i+1,i}(k, k'', s_i \omega) - G_{i+1,i}^*(k'', k, s_i \omega)] \quad (14)$$

Here $G(k_1, k_2, \omega)$ is obtained by analytical continuation $i\omega_n \rightarrow \omega + i\delta$ of $G(k_1, k_2, i\omega_n)$ from imaginary frequencies to real frequencies. The complexity of the above formula stems from translational symmetry breaking in the presence of DDW order.

III. NUMERICAL CALCULATION AND DISCUSSION

We compute the local density of states $\rho(q, \omega)$ using the 4×4 impurity scattering matrices. For potential

scattering given by a δ -function, they are

$$V(k, k') = V_N \begin{pmatrix} 1 & 1 & 0 & 0 \\ 1 & 1 & 0 & 0 \\ 0 & 0 & -1 & -1 \\ 0 & 0 & -1 & -1 \end{pmatrix}. \quad (15)$$

for a non-magnetic impurity, and

$$V(k, k') = V_M \begin{pmatrix} 1 & 1 & 0 & 0 \\ 1 & 1 & 0 & 0 \\ 0 & 0 & 1 & 1 \\ 0 & 0 & 1 & 1 \end{pmatrix}. \quad (16)$$

for a magnetic impurity.

The results are reported for the representative values: $V_N = V_M = 0.1$ eV. For the band dispersion, we choose $t = -1.2$ eV and $t' = 0.36$ eV. The chemical potential is selected to be equal to -0.36 eV. The imaginary part of the energy $\delta = 0.5$ meV is used for the entire numerical calculation. We have checked that the results are unchanged for smaller values of δ . Following Ref. 9, a 400×400 lattice is used in our analysis, and the results are displayed in the $(-\pi, \pi) \times (-\pi, \pi)$ interval on a 49×49 grid for any given frequency. The choice of these parameters is representative. We have repeated our calculations for a number of different set of parameters; the conclusions remain unchanged.

A. The DSC state

First we analyze the interference patterns in a pure superconducting state with $\Delta_0 = 25$ meV. This has also been studied in Ref. 9 for a different bare band structure. The constant energy contour plots are shown in the Fig. 1(b) where we label the wavevectors, which are expected to be associated with the peaks in the interference patterns. In Fig. 2, we show a comparison between our results and the results in Ref. 9, where a different band structure¹³ which is flatter near $(\pi, 0)$ is used. Some of

the features in our results are the same as in Ref. 9, but there are also several clear differences.

For the case of a nonmagnetic impurity, the peaks associated with the wavevectors numbered 3, 4, and 7 are observed for a large energy range. However, the intensity is high mainly along the diagonal or symmetrically about the diagonal, contrary to the results in Ref. 9, where regions of high intensity emerge along the $(0, \pm 1)$ and $(\pm 1, 0)$ directions when the energy $|\omega|$ reaches 15meV. The peak associated with the wave vector numbered 1 appears for some energies, but with weaker intensity than the peaks associated with the above three wave vectors.

For the case of a magnetic impurity, there are fewer features, so it is more difficult to relate the observed intensity to the scattering from the tips of the banana-shaped contours.

B. The mixed DSC and DDW state

If DDW order is the origin of the pseudogap phase, the mixed state should describe the underdoped cuprates at low temperatures. In Fig. 1(d) we sketch the equal energy contours for the band structure of a mixed DDW-DSC state. For energies lower than the DSC gap the equal energy contours are now four pairs of bananas due to the doubling of unit cell by the DDW order, and the regions of high DOS are situated at their tips. However, for energies larger than the DSC gap, the equal energy contours become elliptical, which is characteristic to the DDW state.

In Fig. 3, we plot our results for the mixed state for nonmagnetic impurity scattering. We note that for energies lower than the DSC gap, we can identify exact features characteristic to the pure DSC state. The patterns are almost identical to those obtained in a pure DSC state with the same DSC gap Δ_0 . In particular the peaks along the (π, π) axis disperse with energy in the expected fashion. However, they reach the corners of the BZ at energy comparable to the DSC order parameter Δ_0 , and not to the full gap of the system $\Delta_t = \sqrt{W_0^2 + \Delta_0^2}$. Above the energy Δ_0 , a whole range of different features emerge, which are characteristic to the DDW state. For comparison, in Fig. 4 we plot the corresponding results for the case of a pure DSC state with a gap equal to the total gap of the mixed state Δ_t . Indeed, the peaks in the pure DSC state disperse much slower with energy and can be observed at higher energies than in the mixed state. Based on these observations we expect the FT-STs measurements to be an experimental tool to observe the coexistence of DDW order with DSC order in the underdoped cuprates. If this state is indeed a coexisting DDW and DSC state, measurements done at various energies should reveal that the diagonal peaks in the spectra should approach the corners of the BZ well before the full gap is reached. Also, entirely new features should arise in the STM spectra for energies above the energy for which the peaks have reached the corners. The new features

would be similar to what one would expect to see in a pure DDW state. Broad regions of high intensity are expected rather than sharp peaks, as we will discuss in the next subsection. When the doping is increased, since the total gap Δ_t is roughly constant for different doping levels, the DDW gap decreases and the DSC gap increases. The energy at which the transition described above happens in the interference patterns is thus expected to get closer and closer to the total gap and eventually equal to it when the DDW gap vanishes and the DDW ordering disappears.

C. The DDW state

We now turn to a pure DDW state. In Fig. 1(c) we plot a typical band structure of a pure DDW state. We note that the equal energy contours are now elliptical and we therefore expect the high DOS regions to be situated at their tips, though, due to the smaller curvature of these contours, the distinction between the high and low regions of DOS are not as strong as in the case of DSC. In Fig. 5, we plot the corresponding LDOS results for $W_0 = 25$ meV, and $W_0 = 40$ meV.

Even though one can still track the presence of peaks, they are not as pronounced. This may be the result of a more uniform DOS. The position of some of the peaks (such as some along the (π, π) direction and symmetrically about it, and some along the $(\pi, 0)$ direction) may be traced back to the positions of the tips of the elliptical contours in the band structure. These peaks are present in most of the pictures, but their intensities vary.

Also, for the chosen band structure, peaks located around $(\pm \frac{\pi}{4}, 0)$ and $(0, \pm \frac{\pi}{4})$ can be found over a broad range of energy. They are present in both the $W_0 = 40$ meV and $W_0 = 25$ meV data. In particular, their positions hardly change with energy for positive energies. We note that their peculiar positions of roughly $(\pm \frac{\pi}{4}, 0)$ and $(0, \pm \frac{\pi}{4})$ is an effect of the particular set of parameters in the band structure. The origin of these peaks is the scattering indicated by the arrow in Fig. 1(c). Since the equal energy contours may change drastically with a change of parameters, so may the position of the peaks. We also note that, since the equal energy contours change very little with energy for positive energies, the peaks also do not move when the energy is varied.

Many other peaks however cannot be explained by simple band structure arguments, and their positions change drastically from one plot to the next.

The predominant feature for the DDW state is thus the presence of broadly distributed scattering points in the interference patterns at low energy. However, lines with relatively high intensity are also present in our data. Such lines actually occur in all of the states considered. Furthermore, the intensity and size of these lines vary strongly with even slight changes of parameters. This is in contrast to the statement in Ref. 11 that the presence of high intensity lines in the spectrum is a characteristic

of the DDW state. However, since the equal energy contours are elliptical, the scattering patterns in the DDW states are much more likely to be affected by coherence factors than the scattering patterns in other states. Because of this effect, the comparison between DDW and DSC in Ref. 11, based on Born approximation, should not be considered as generic, although we generally agree that the interference patterns are different in these states. We will discuss this in more detail in the next subsection.

As a final observation, we note that if we tune the parameters such that electron pockets around $(\pm\pi, 0)$ and $(0, \pm\pi)$ appear in the DDW band structure, our calculation shows circles of high intensity in the BZ corresponding to electrons with different momenta scattering off each other. This appears to be the dominant feature. However, the presence of such electron pockets is not consistent with ARPES data¹⁴ and we do not include the results for this situation in the present work.

D. Discussion of the coherence factors

The interference patterns not only depend on the band structure and on the order parameters, but also on the coherence factors. This dependence on coherence factors has quite complex effects and makes the interference patterns sensitive to many details.

First, the coherence factors depend on the strength and the type of the impurity scattering. In Ref. 9, the interference patterns from nonmagnetic and magnetic impurities were shown to be so different that entirely different peaks were observed, even for pure s -wave scattering. Clearly, similar or more pronounced effects may arise in the case of non s -wave scattering. Furthermore, the coherence factors depend on the impurity scattering strength. This may be implied from the sensitivity of the interference patterns to whether we use the Born approximation or a full T-matrix calculation for a reasonable impurity strength.

Second, the coherence factors are also strongly sensitive to the band structure and order parameters. The band structure dependence causes the dramatic difference between our results for the DSC state and the results in Ref. 9. The flatness of the band structure of Ref. 13 leads to differences in the DOS and also to important differences in the coherence factors. In the DDW state, the effect of coherence factors is more dramatic than in the DSC states, as seen from the plot of our results for identical parameter sets save for the DDW gaps. Though the band structures for the two chosen DDW gaps are very similar, as seen in Fig. 5 there are considerable differences between the corresponding FT-STs patterns.

Third, the coherence factors are sensitive to energy. This has been shown consistently in all our calculations. Even for similar band structures, some peaks can only be identified for some ranges of energy, while others appear or disappear in a manner counterintuitive to expectations

based on band structure.

Finally, the coherence factors should also be expected to depend on the correlation and distribution of impurities in the materials.

The sensitivity of the coherence factors to so many details makes it difficult to extract information about the dispersion of quasiparticles from the interference patterns. It is rather hard to identify a feature that can be traced in a broad energy range. This is particularly true for the DDW state, where the quasiparticle scattering interference is much more sensitive to the changes of the parameters in the model.

IV. CONCLUSIONS

In this paper we have analyzed the effects of scattering from a single impurity on FT-STs in a high T_c superconductor with DDW ordering. For the case of a pure superconducting state, we recovered results similar to Ref. 9. We note the presence of peaks dispersing with energy in the expected fashion. However, some important features are strongly dependent on the band structure and on other parameters in the model even if the banana-shaped equal-energy plots are similar. In the case of a mixed DDW-DSC state, we note that the DSC order dominates the interference patterns at energies lower than the DSC gap Δ_0 , while for higher energies, a transition to a spectra characteristic of the DDW phase occurs. This is marked by a sudden change of the general features of the STM spectra around an energy $E = \Delta_0$. In particular, we show that the dispersion of the diagonal peaks in the spectrum can be used to identify this transition. In the underdoped regime, the DSC gap Δ_0 is reduced when the doping decreases, so the energy at which the transition happens should also be reduced. Based on this observation, we predict that the STM measurements in the underdoped cuprates below T_c may reveal important information about the nature of the gap. In the pure DDW state the results are more complex; the peaks are more broadly spaced and not so pronounced and are more sensitive to changes of parameters. It would be interesting to see if STM experiments in the pseudogap regime can provide new insight into the problem.

V. ACKNOWLEDGMENTS

C. B. has been supported by the NSF under Grant No. DMR-9985255, and also by funds from the A. P. Sloan Foundation and the Packard Foundation. S. C. has been supported by the NSF under Grant No. DMR-9971138. JP was supported by the funds from the David Saxon chair at UCLA. C. N. has been supported by the NSF under Grant No. DMR-9983544 and the A.P. Sloan Foundation.

-
- ¹ T. Timusk and B. Statt, Rep. Prog. Phys. **62**, 61 (1999).
- ² S. Chakravarty, R. B. Laughlin, D. K. Morr, and C. Nayak, Phys. Rev. B **63**, 4503 (2001).
- ³ H. J. Schulz, Phys. Rev. B **64**, 2940 (1989); I. Affleck and J. B. Marston, Phys. Rev. B **37**, 3774 (1988); G. Kotliar, Phys. Rev. B **37**, 3664 (1988); D. A. Ivanov, P. A. Lee, and X.-G. Wen, Phys. Rev. Lett. **84**, 3958 (2000); C. Nayak, Phys. Rev. B **62**, 4880 (2000).
- ⁴ J. E. Hoffman, K. McElroy, D.-H. Lee, K. M. Lang, H. Eisaki, S. Uchida, and J. C. Davis, Science **297**, 1148 (2002).
- ⁵ K. McElroy, R. W. Simmonds, J. E. Hoffman, D.-H. Lee, J. Orenstein, H. Eisaki, S. Uchida, J. C. Davis, Nature **422**, 592 (2003).
- ⁶ C. Howald, H. Eisaki, N. Kaneko, M. Greven, and A. Kapitulnik, Phys. Rev. B **67**, 014533 (2003).
- ⁷ J. M. Byers, M. E. Flatté and D. J. Scalapino, Phys. Rev. Lett. **71**, 3363 (1993).
- ⁸ M. E. Flatté and J. M. Byers, Phys. Rev. Lett. **80**, 4546 (1998).
- ⁹ Q.-H. Wang and D. H. Lee, Phys. Rev. B **67**, 020511 (2003).
- ¹⁰ L. Capriotti, D.J. Scalapino, and R.D. Sedgewick, Phys. Rev. B, to be published (cond-mat/0302563).
- ¹¹ T. Pereg-Barnea and M. Franz, cond-mat/0306172.
- ¹² J. R. Schrieffer, Theory of Superconductivity, W. A. Benjamin inc. publishers, New York, 1964.
- ¹³ M. R. Norman, M. Randeria, H. Ding, J. C. Campuzano, Phys. Rev. B **52**, 615 (1994).
- ¹⁴ A. G. Loeser, *et al.*, Science **273**, 325 (1996); H. Ding, *et al.*, Nature **382**, 51 (1996).

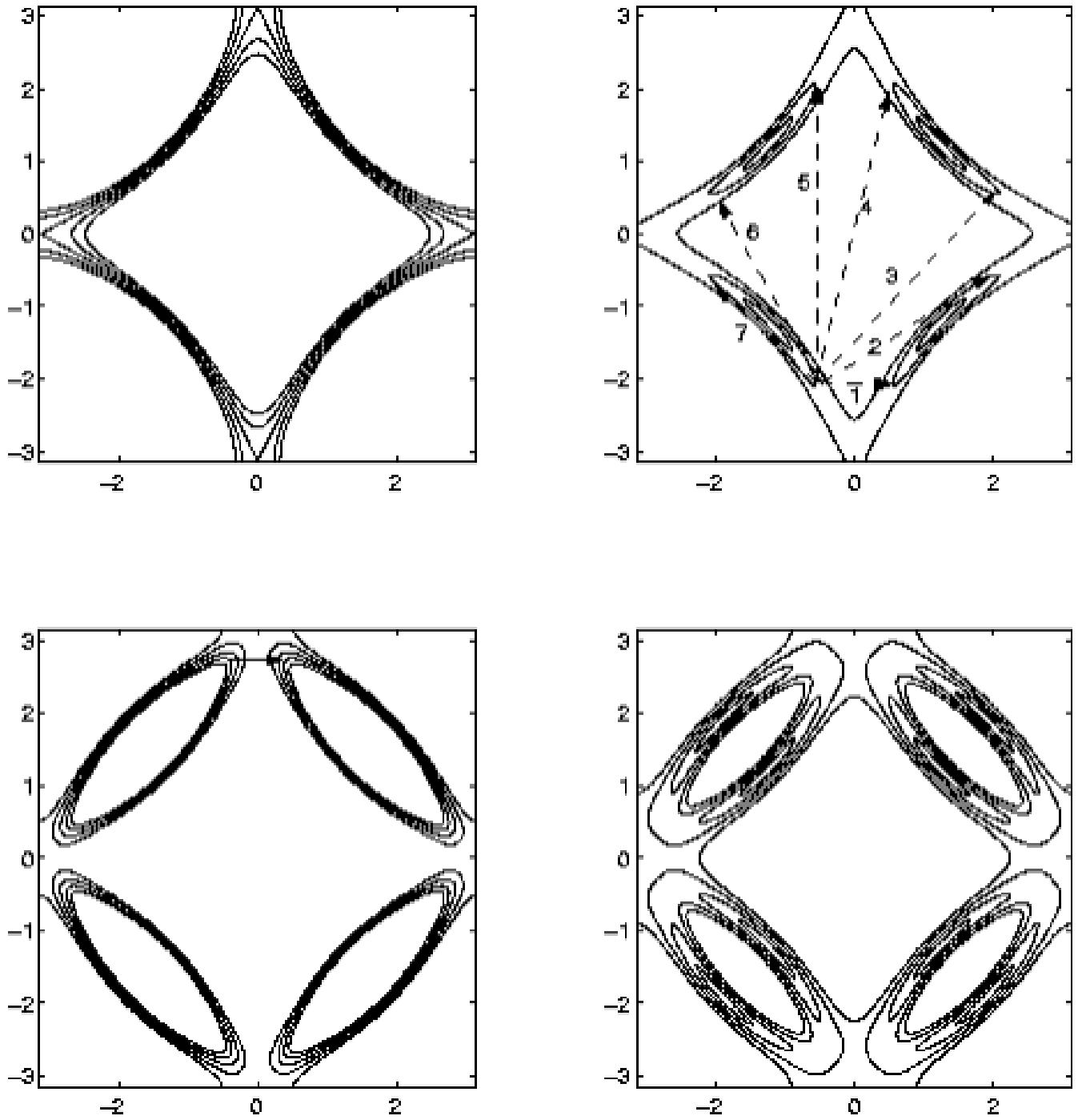


FIG. 1: Equal energy contour plots in different states: (a) normal state without any order, (b) d -wave superconducting state (DSC), (c) d -density wave state (DDW), and (d) Mixed DSC and DDW state (DSC-DDW).

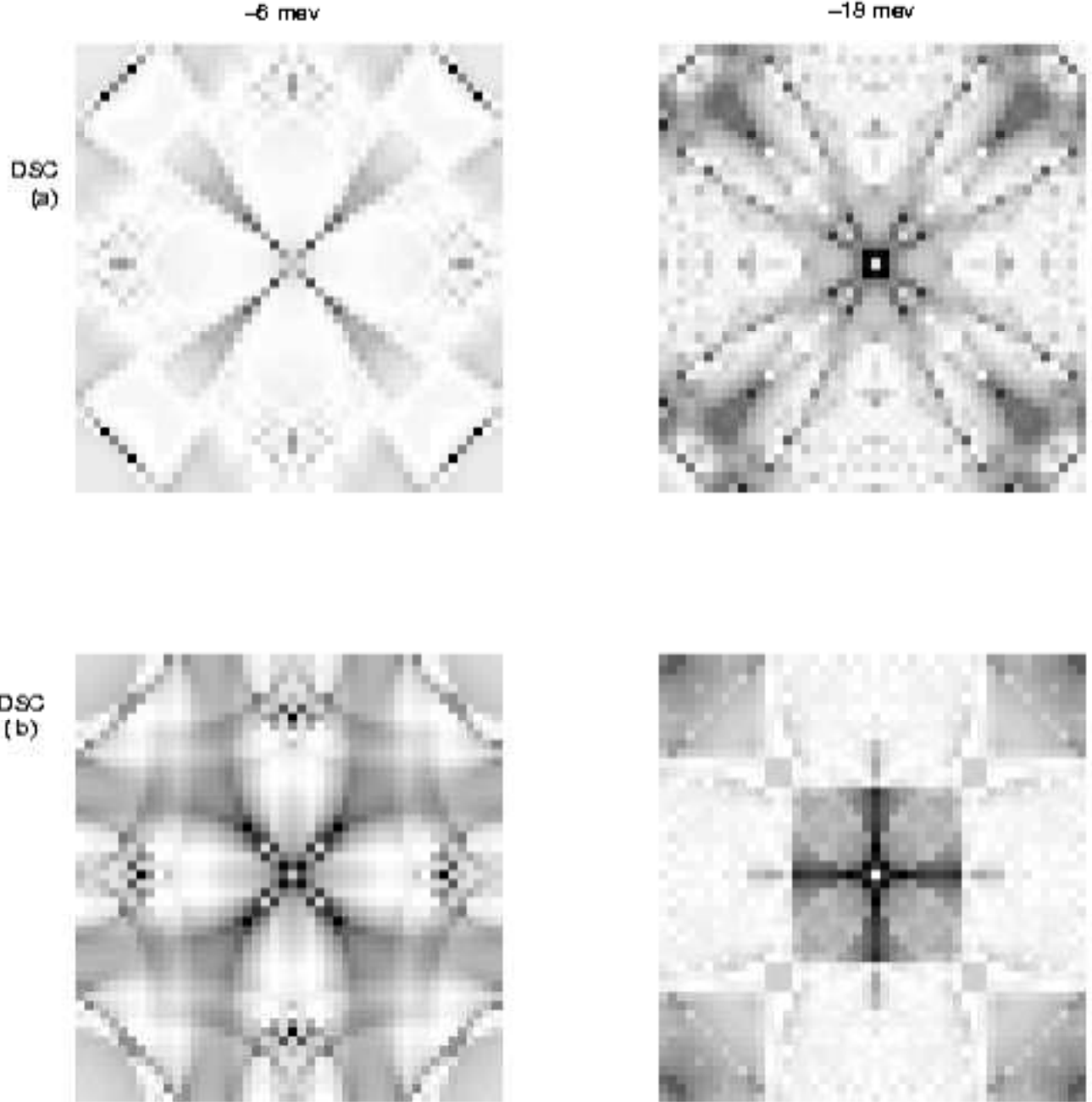


FIG. 2: Fourier transform of STM spectra: (a) in a pure DSC state with the $t - t'$ band structure and $\Delta_0 = 25$ meV, (b) in a pure DSC state with the band structure in Ref. 13 and $\Delta_0 = 25$ meV and at energies equal to -6 meV and -18 meV, for nonmagnetic impurity scattering ($V_N = 100$ meV). The differences between (a) and (b) reflect the sensitivity of FT-STs spectra to band structure details.

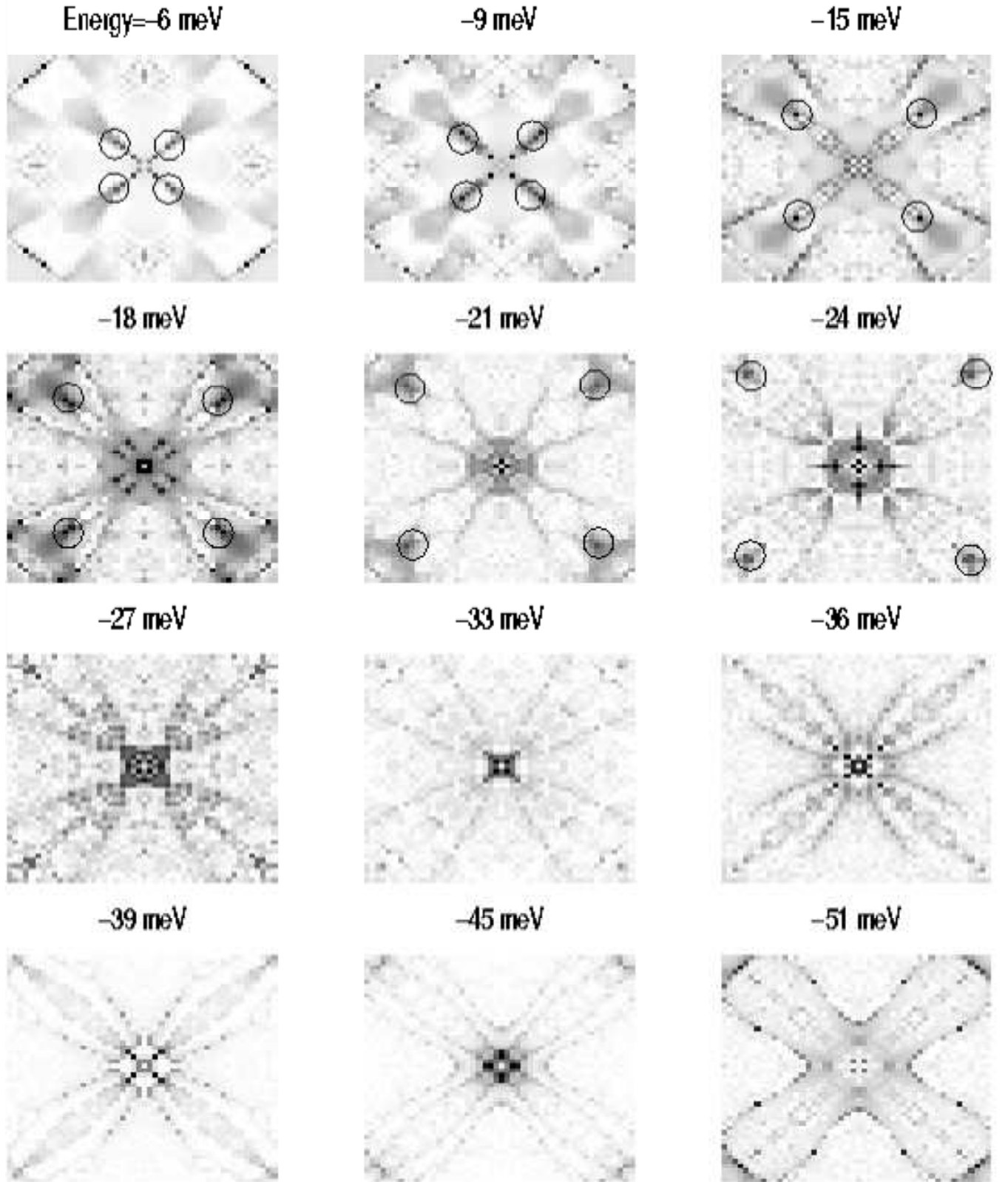


FIG. 3: Fourier transform of STM in the coexisting DSC-DDW state with the $t - t'$ band structure, $\Delta_0 = 25\text{meV}$ and $W_0 = 40\text{meV}$, for nonmagnetic impurity scattering ($V_N = 100\text{meV}$). The peaks along the directions $(\pm\pi, \pm\pi)$ are marked by circles. As noted, these peaks get close to the corners of the BZ at energies equal to the DSC gap Δ_0 , and not to the total gap, which is $\Delta_t \approx 47\text{meV}$. Also, the general features of the spectra change dramatically at energies larger than Δ_0 .

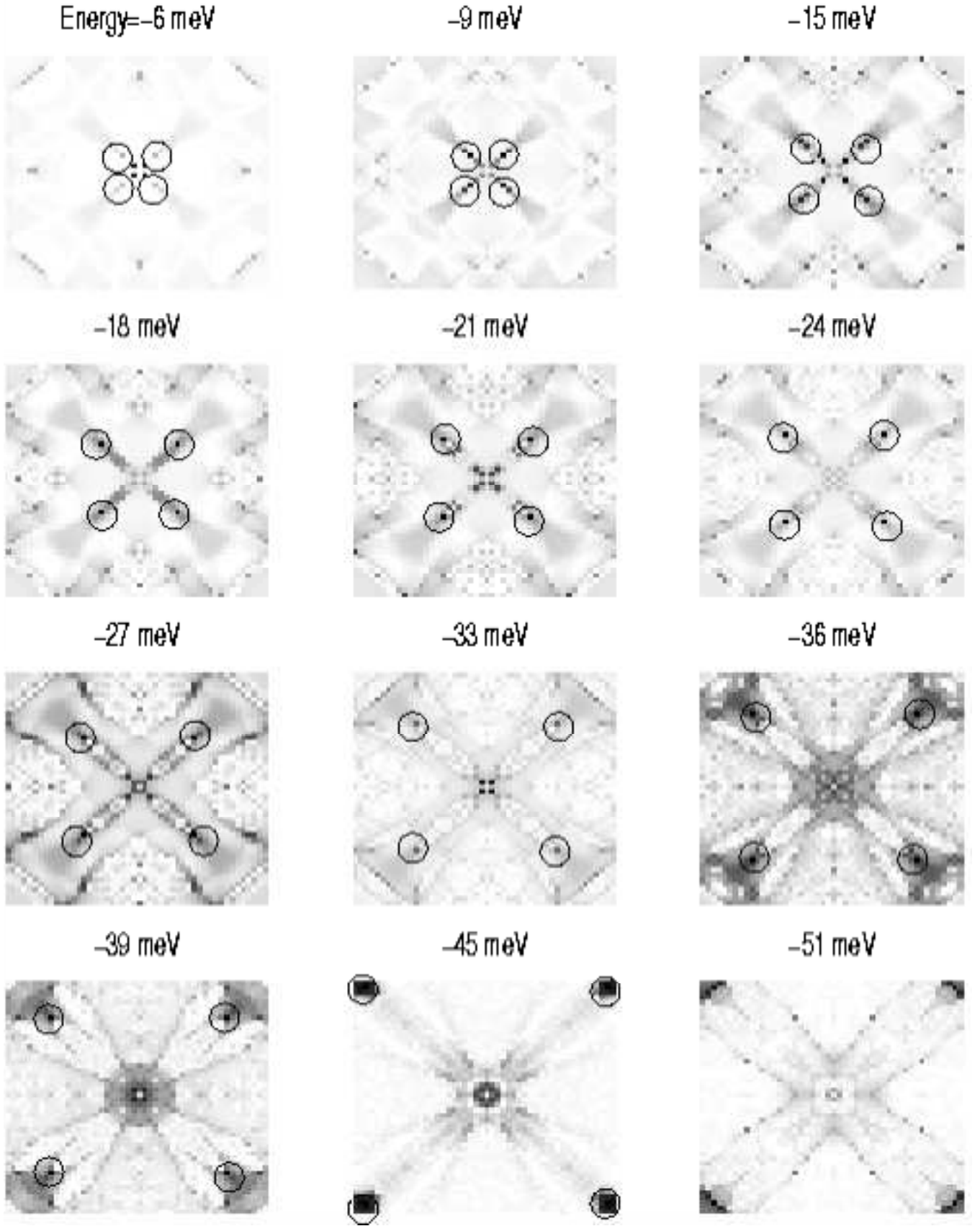


FIG. 4: Fourier transform STM spectra in a pure DSC state with the $t - t'$ band structure and $\Delta_0 = 47\text{meV}$, for nonmagnetic impurity scattering $V_N = 100\text{meV}$. Again, the peaks along the directions $(\pm\pi, \pm\pi)$ are marked by circles. In this case, the peaks get close to the corners of the BZ for energies equal to the DSC gap $\Delta_0 = 47\text{meV}$.

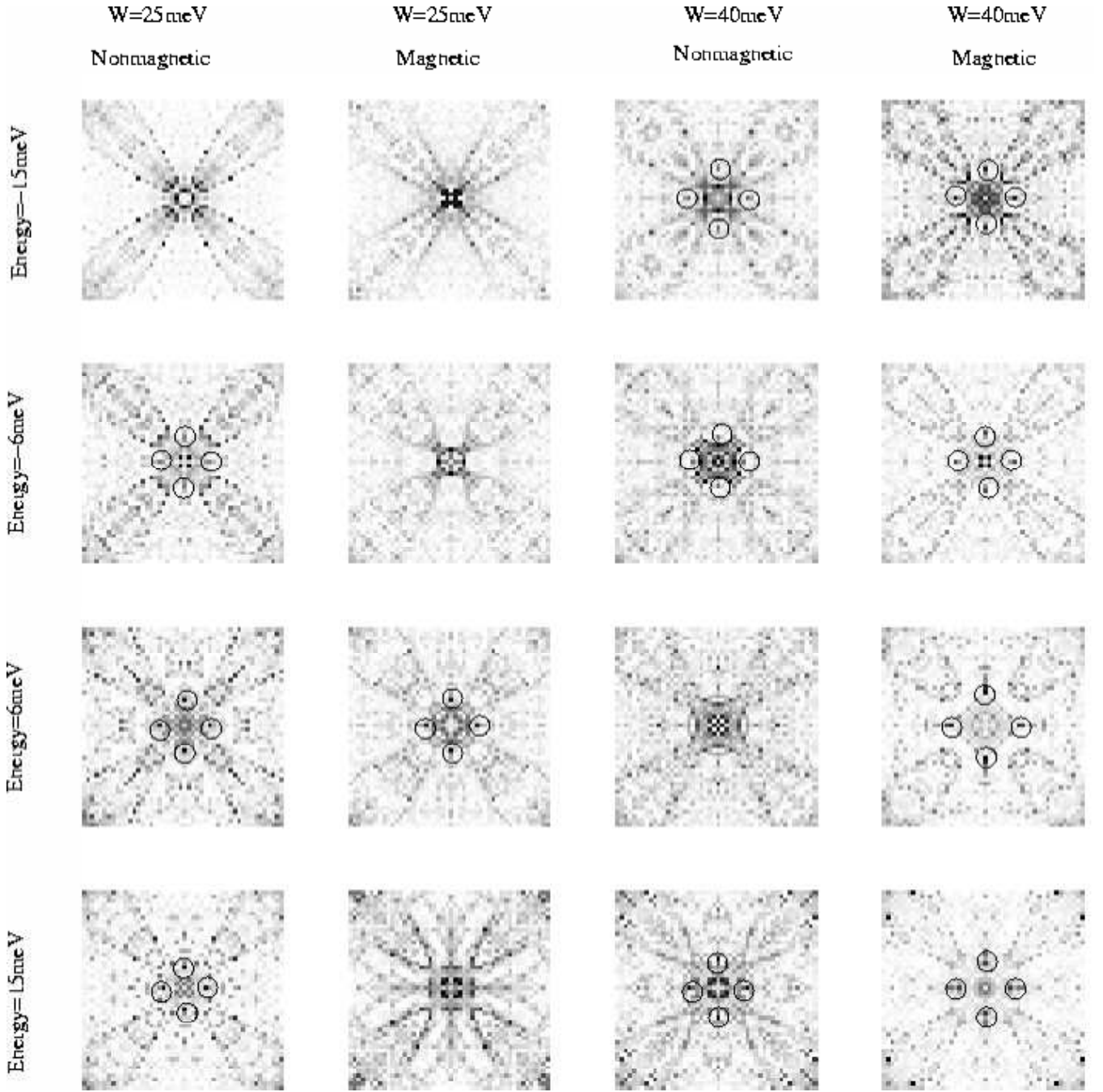


FIG. 5: Fourier transform STM spectra in the pure DDW state with the $t - t'$ band structure and $W_0 = 40\text{meV}$, for non-magnetic ($V_N = 100\text{meV}$) and magnetic ($V_M = 100\text{meV}$) impurity scattering. The peaks at $(0, \pm\pi/4)$ and $(\pm\pi/4, 0)$ are marked by circles and can be observed for a large range of energies.